Reconstructing the parameter space of non-analytical cosmological fixed points

Santiago García-Serna,* J. Bayron Orjuela-Quintana,[†] César A. Valenzuela-Toledo,[‡] and Hernán Ocampo Durán[§] Departamento de Física, Universidad del Valle, Ciudad Universitaria Meléndez, Santiago de Cali 760032, Colombia

Dynamical system theory is a widely used technique to analyze the asymptotic behavior of a cosmological model. In this method, the equations that describes the dynamics are written in terms of dimensionless variables to make up a set of autonomous first-order differential equations. Then, the asymptotic dynamics of the model are encoded in the fixed points of the autonomous set. Usually, these points are analytical expressions for the variables in terms of the parameters of the model, allowing us to constrain its parameter space. However, analytical treatment could be impossible in some cases. In this work, we give an example of a dark energy (DE) model with no analytical fixed points, a tachyon field coupled to a vector field in an anisotropic Bianchi I background, and propose a numerical description of the parameter space, which allows us to find the bifurcation curves of possible accelerated attractors of the system. This work could serve as a template for numerical analysis of highly complicated dynamical systems.

PACS numbers: 98.80.Cq; 95.36.+x

I. INTRODUCTION

Since the discovery of the accelerated expansion of the Universe at the end of the past century [1–3], a wealth of observations have established the Λ CDM model as the most simple and accurate model that describes the evolution of the Universe from the Big-Bang to present days [4–11]. However, some pretty interesting discrepancies, such as the H_0 and σ_8 tensions [12–23], or the CMB anomalies [24–28], are challenging this paradigm. These cosmological tensions have provided a further motivation to explore theoretical alternatives to the concordance model [29–32].

On the other hand, one of the most powerful tools to analyze the viability of a theoretical proposal is the dynamical system technique [33–35]. When applied in cosmology, this technique basically consists in writing the field equations in terms of dimensionless variables which are, typically, chosen by writing the first Friedman equation as an algebraic constraint. This yields to a set of autonomous first order differential equations whose stationary solutions can be found in the compact space for the dynamical variables, ¹ which schematically can be represented as

$$x_i' = f_i(x_1, \dots, x_n | a_1, a_2 \dots),$$
 (1)

where a prime denotes derivative with respect to the number of e-folds, and f_i is an algebraic expression in terms of the n variables x_j and k parameters a_j . The number of parameters clearly depends on the specific theory. The asymptotic behavior of the system is encoded in the stability of the fixed points of the autonomous set. These fixed points define the possible stationary states of the system, therefore, they can be found by doing $x'_i = 0$, for each variable. This yields to a set of algebraic equations in terms of the parameters of the model, whose solutions allow us to constraint the available parameter space of the model. This technique as described has been widely used in cosmology (see for example Refs. [39–45]).

Usually, the resulting set of algebraic equations is analytically solvable using softwares for symbolic computation, for instance, using the command Solve in Mathematica. However, there are two main reasons this computational strategy is not always applicable: i) the set is too complicated or ii) analytic solution simply do not exist (see for example Refs. [46, 47]).

In this work, we propose a numerical method to find the fixed points of an autonomous set. Given an initial window parameter, our method is able to find the bifurcation curve separating possible attraction regions of the system. We illustrate our method in an anisotropic dark energy (DE) model based on the dynamics of a scalar tachyon field. This work is complemented with a full numerical solution of the autonomous set to ensure that the asymptotic cosmology is in agreement with the predictions given by the numerical fixed points.

This paper is organized in the following way. In section II, we present a general overview of our numerical

^{*} santiago.serna@correounivalle.edu.co

[†] john.orjuela@correounivalle.edu.co

 $^{^{\}ddagger}$ cesar.valenzuela@correounivalle.edu.co

 $[\]S$ hernan.ocampo@correounivalle.edu.co

¹ A compact space is not a requirement in general. However, it is indeed a desirable feature since it ensures the existence of a global repeller and a global attractor [36–38].

implementation of dynamical systems. In section III, we illustrate our numerical method applying it to a particular cosmological model. A full numerical solution of the autonomous set is presented in Sec. IV. Finally, our conclusions are presented in the section V.

II. DYNAMICAL SYSTEMS: NUMERICAL APPROACH

In this section, we describe how the cosmological parameter space of a model can be found. Assuming that we have an autonomous system of n equations as in Eq. (1), our method relies in the following steps:

1. Choice of a representative region in the parameter space of the model.

The simplest region we can choose has the form $a_{i_{\min}} < a_i < a_{i_{\max}}$ for $i=1,2,\ldots$. As we will show in the next section, we can take into consideration the symmetries of the autonomous system and analytical solutions of a simplified autonomous system in order to choose the bounds $a_{i_{\min}}$ and $a_{i_{\max}}$ based on physical arguments.

2. Physical constraints to discriminate between viable and non-viable points in the parameter space.

For instance, these physical constraints can be the requirements that the density parameters are positive and bounded by 1, or that the solution implies accelerated expansion of the Universe.

Stochastic search of physical points in the chosen region.

We generate a large number N of random points in the parameter space $\{a_1, a_2, \ldots\}$ and, for each point, we find the corresponding fixed points by solving the n algebraic equations $f_i = 0, i = 1, \ldots, n$ numerically.² Then, we discriminate each solution evaluating whether the physical constraints are fulfilled or not. If a solution obeys all the physical constraints, we say that we have obtained a "viable point" in the parameter space. Otherwise, we have obtained a "non-viable point". In the case when the model has two parameters, the stochastic search can yield to results schematically similar to the region plotted in

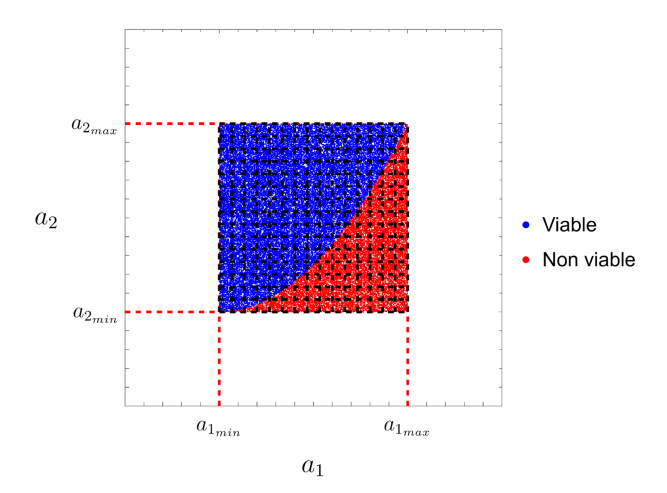


FIG. 1. Parameter space where a stochastic search for viable and non-viable points has been performed.

Fig. 1. In our case of interest, all the viable solutions will correspond to DE dominated points since the radiation and matter dominated points can be found analytically.

4. Stability analysis of the region of viable points.

In general, the stability of a fixed point can be determined by computing the real part of the eigenvalues of the Jacobian matrix evaluated in the point.³ When all the corresponding eigenvalues are negative, we say that the fixed points is an attractor. When all of them are positive, the fixed point is a source. But if there is a mix of negative and positive eigenvalues, then the fixed point is a saddle.

In the cosmological context, a proper expansion history requires the existence of at least three fixed points as follows: i) a radiation dominated point which can be a saddle or a source, ii) a saddle matter dominated point, and iii) a DE dominated point as the only attractor of the system.

Note that for a given point in the parameter space, there could exist several fixed points with their own stability. Therefore, we have to compute all the available Jacobian matrices (and their eigenvalues) for each set of parameters. However, since we are mainly interested in DE dominated points, we prioritize the search of attractors, such that once an attractor is found, the computation of the Jacobian matrices for

² This can be done using the default numerical methods in the NSolve of Mathematica, for example.

³ The Jacobian matrix for a dynamical system with n equations of the form $x_i' = f(x_1, \ldots, x_n)$ is defined as $J_{ij} = \frac{\partial x_i'}{\partial x_j}$.

the given set of parameters is stopped, just to proceed to another point in the parameter space. We want to stress that we prioritize attractors since we are interested in DE dominated points. However, this approach can be easily generalized to search source or saddle points.

In the following section, we will illustrate the numerical method described here by analyzing the asymptotic behaviour of a specific model.

III. ILLUSTRATION OF THE METHOD

A. Tachyon field in an anisotropic background

The Lagrangian of the model is given by

$$S \equiv \int d^4x \sqrt{-g} \left(\mathcal{L}_{EH} + \mathcal{L} + \mathcal{L}_m + \mathcal{L}_r \right), \quad (2)$$

where $\mathcal{L}_{EH} \equiv M_{Pl}^2 R/2$, M_{Pl} is the reduced Planck mass, R is the Ricci scalar, \mathcal{L}_m and \mathcal{L}_r are the Lagrangians for matter and radiation, respectively, and

$$\mathcal{L} \equiv -V(\phi)\sqrt{1 + \partial_{\mu}\phi\partial^{\mu}\phi} - \frac{1}{4}f(\phi)F^{\mu\nu}F_{\mu\nu}, \quad (3)$$

where ϕ is the scalar tachyon field, $V(\phi)$ is its potential, $F_{\mu\nu} \equiv \nabla_{\mu}A_{\nu} - \nabla_{\nu}A_{\mu}$ is the strength tensor associated to the vector field A_{μ} , and $f(\phi)$ is a coupling function between ϕ and A_{μ} . Next, we assume that the background geometry is described by a Bianchi I metric with rotational symmetry in the y-z plane, such as the line element is written as

$$ds^{2} = -dt^{2} + a^{2}(t) \left[e^{-4\sigma(t)} dx^{2} + e^{2\sigma(t)} \left(dy^{2} + dz^{2} \right) \right],$$
(4)

where a(t) is the average scale factor and $\sigma(t)$ is the geometrical shear, being both functions of the cosmic time t. In order to preserve the symmetries of the background, we choose the field profiles as

$$\phi \equiv \phi(t), \quad A_{\mu} \equiv (0, A(t), 0, 0),$$
 (5)

being A(t) an scalar field and the only component of the vector field.

We want to make a few comments about the specific model we study here. Firstly, a dynamical system analysis of the tachyon field can be found in the literature, Refs. [48–52] are some examples. All these works get analytical results. However, as pointed out in Refs. [46] and [47], a full analytical description of the dynamical system is impossible for some non-canonical scalar field models in a Bianchi-I background, such as the Dirac-Born-Infeld (DBI) field. Since the Lagrangian of the DBI model shares some

similarities with the Lagrangian in Eq. (3), we expect that the dynamical system of this model also lacks of a full analytical description. We will explicitly show that the anisotropic dark energy attractor of the tachyon field model cannot be studied analytically and use the numerical method explained in Sec. II to reconstruct its parameter space.

B. Dynamical System

In the following, we will present the field equations of the model as a dynamical system.

Following the standard procedure, we derive the evolution equations of the model by varying the action in Eq. (2) with respect to the metric, the scalar field and the vector field. After the variation, we replace the Bianchi I metric given in Eq. (4), and the ansatz for the fields in Eq. (5). obtaining:

$$3M_{\rm Pl}^2 H^2 = \frac{1}{2} f \frac{e^{4\sigma} \dot{A}^2}{a^2} + \frac{V}{\sqrt{1 - \dot{\phi}^2}} + \rho_m + \rho_r + 3M_{\rm Pl}^2 \dot{\sigma}^2.$$
 (6)

$$-2M_{\rm Pl}^2 \dot{H} = \dot{\phi}^2 \frac{V}{\sqrt{1 - \dot{\phi}^2}} + \frac{2}{3} f \frac{e^{4\sigma} \dot{A}^2}{a^2} + \frac{4}{3} \rho_r + \rho_m + 6M_{\rm Pl}^2 \dot{\sigma}^2,$$
(7)

$$\ddot{\sigma} + 3H\dot{\sigma} = \frac{e^{4\sigma}f\dot{A}^2}{3a^2M_{\rm Pl}^2},\tag{8}$$

$$\frac{\ddot{\phi}}{1 - \dot{\phi}^2} = \frac{\sqrt{1 - \dot{\phi}^2} f_{,\phi}}{2V a^2} e^{4\sigma} \dot{A}^2 - \frac{V_{,\phi}}{V} - 3H\dot{\phi}, \quad (9)$$

$$\frac{\ddot{A}}{\dot{A}} = -\frac{\mathrm{d}}{\mathrm{d}t} \ln\left(afe^{4\sigma}\right),\tag{10}$$

where H is the Hubble parameter, ρ_r and ρ_m are the densities of matter and radiation, respectively, and a dot indicates derivative with respect to t. Equations (6) and (7) correspond to the first and second Friedman equations, Eq. (8) is the evolution equation for the geometrical shear, and Eqs. (9) and (10) are the equations of motion for the scalar and vector fields, respectively. The above equations can be recast in terms of the following dimensionless variables

$$x \equiv \dot{\phi}, \quad y^2 \equiv \frac{V(\phi)}{3M_{\rm Pl}^2 H^2}, \quad z^2 \equiv \frac{1}{2} f(\phi) \frac{e^{4\sigma} \dot{A}^2}{3M_{\rm Pl}^2 H^2 a^2},$$
$$\Omega_m \equiv \frac{\rho_m}{3M_{\rm Pl}^2 H^2}, \quad \Omega_r \equiv \frac{\rho_r}{3M_{\rm Pl}^2 H^2}, \quad \Sigma \equiv \frac{\dot{\sigma}}{H}. \quad (11)$$

The first Friedman equation in Eq. (6) becomes the

constraint

$$1 = \frac{y^2}{\sqrt{1 - x^2}} + z^2 + \Sigma^2 + \Omega_m + \Omega_r, \qquad (12)$$

while from Eq. (7) we can compute the deceleration parameter $q \equiv -1 - \dot{H}/H^2$ obtaining

$$q = \frac{1}{2} \left[1 - 3\sqrt{1 - x^2}y^2 + z^2 + \Omega_r + 3\Sigma^2 \right].$$
 (13)

We can easily integrate Eq. (10) such that for the vector field degree of freedom we have

$$\dot{A} = c \frac{e^{-4\sigma}}{af},\tag{14}$$

where c is a constant. From the Friedman equations (6) and (7), we can identify the density and pressure of dark energy, which can be written in terms of the dimensionless variables as

$$\rho_{\rm DE} \equiv 3M_{\rm Pl}^2 H^2 \left(\frac{y^2}{\sqrt{1-x^2}} + z^2 + \Sigma^2 \right),$$
(15)

$$p_{\rm DE} \equiv 3M_{\rm Pl}^2 H^2 \left(-y^2 \sqrt{1-x^2} + \frac{1}{3}z^2 + \Sigma^2 \right), \quad (16)$$

respectively. Now, the equation of state of DE, $w_{\rm DE} \equiv p_{\rm DE}/\rho_{\rm DE}$, is given by

$$w_{\rm DE} = -1 + \frac{2}{3} \frac{\frac{3}{2} \frac{x^2 y^2}{\sqrt{1 - x^2}} + 2z^2 + 3\Sigma^2}{\frac{y^2}{\sqrt{1 - x^2}} + z^2 + \Sigma^2}.$$
 (17)

Note that we included the geometrical shear Σ in the definition of $\rho_{\rm DE}$ and $p_{\rm DE}$. This choice allows us to write the continuity equation of DE as

$$\dot{\rho}_{\rm DE} + 3H(\rho_{\rm DE} + p_{\rm DE}) = 0,$$
 (18)

which is the usual form of the continuity equation, stressing that we are considering that DE can be an anisotropic fluid.

In order to calculate the evolution equations for the dimensionless variables, we differentiate each variable in Eq. (11) with respect to the number of e-folds.⁴

We get

$$x' = \sqrt{3} (1 - x^2) \left[\frac{\sqrt{1 - x^2}}{y} \beta z^2 - \sqrt{3}x - \alpha y \right],$$
(19)

$$y' = y \left[\frac{\sqrt{3}}{2} \alpha y x + q + 1 \right], \tag{20}$$

$$z' = z(q-1) - 2z\Sigma - \frac{\sqrt{3}}{2}\beta xyz, \tag{21}$$

$$\Sigma' = \Sigma(q-2) + 2z^2,\tag{22}$$

$$\Omega_r' = 2\Omega_r(q-1),\tag{23}$$

where

$$\alpha(t) \equiv M_{\rm Pl} \frac{V_{,\phi}}{V^{3/2}}, \quad \beta(t) \equiv M_{\rm Pl} \frac{f_{,\phi}}{f \sqrt{V}}.$$
 (24)

However, in order to ease computations, we will assume that α and β are constants.

The asymptotic behavior of the system is encoded in the fixed points of the autonomous system in Eqs. (19)-(23). These fixed points are found by doing simultaneously x'=0, y'=0, z'=0, $\Sigma'=0$, and $\Omega'_r=0$. The stability of each point follows from the sign of the real part of the eigenvalues of the Jacobian matrix evaluated at the point. We say that the point is an attractor if all eigenvalues are negative, a saddle if there are positive and negative eigenvalues, and a repeller if all of the eigenvalues are positive.

C. Analytical Fixed points

We can do analytical progress when the anisotropy is neglected. In the following, we study the fixed points relevant for the radiation era ($\Omega_r \simeq 1$, $w_{\rm eff} \simeq 1/3$), the matter era, ($\Omega_m \simeq 1$, $w_{\rm eff} \simeq 0$) and an isotropic DE era ($\Omega_{\rm DE} \equiv \rho_{\rm DE}/3M_{\rm Pl}^2H^2 \simeq 1$, $w_{\rm eff} < -1/3$).

• (R) Radiation dominance:

$$x = 0, y = 0, z = 0, \Sigma = 0, \Omega_r = 1,$$
 (25)

with $\Omega_{\rm DE}=0$, $w_{\rm DE}=-1$, $\Omega_m=0$ and $w_{\rm eff}=1/3$. The eigenvalues of the Jacobian evaluated in this point are

$$2, -1, 1, 0, -3.$$
 (26)

Therefore, (R) is a saddle.

• (M) Matter dominance:

$$x = 0, y = 0, z = 0, \Sigma = 0, \Omega_r = 0,$$
 (27)

 $^{^4}$ The relation between the number of e-folds and the scale factor is $N=\ln a.$

with $\Omega_{\rm DE}=0$, $w_{\rm DE}=-1$, $\Omega_m=1$ and $w_{\rm eff}=0$. The eigenvalues of the Jacobian evaluated in this point are

$$-\frac{3}{2}$$
, $\frac{3}{2}$, -1 , $-\frac{1}{2}$, -3 . (28)

Then, this point is a saddle.

• (*DE-1*) Isotropic DE dominance:

$$x = \mp \frac{\alpha \sqrt{\sqrt{36 + \alpha^4 - \alpha^2}}}{3\sqrt{2}}, \quad \Sigma = 0,$$

$$y = \pm \frac{\sqrt{\sqrt{36 + \alpha^4 - \alpha^2}}}{\sqrt{6}}, \quad z = 0,$$
 (29)

with $\Omega_{\rm DE}=1,\,\Omega_m=0,\,\Omega_r=0$ and

$$w_{\rm DE} = -1 + \frac{1}{18}\alpha^2 \left(-\alpha^2 + \sqrt{36 + \alpha^4}\right).$$
 (30)

Since $w_{\rm DE} = w_{\rm eff}$ in this point, the condition for accelerated expansion ($w_{\rm eff} < -1/3$) is satisfied when $|\alpha| < 3^{1/4}\sqrt{2} \approx 1.86121$.

In this case, the eigenvalues are very long quantities which we present in Appendix A. From those expressions we see that just one eigenvalue depends on α and β , while the remaining four eigenvalues depend on α . In Fig. 2 we see that $\lambda_{1,2,3,4} < 0$ in the region where (DE-I) is an accelerated solution. In Fig. 3, we plot λ_5 in the same interval for α as in Fig. 2 and we choose $\beta \in [-30,30]$ as a representative region for this parameter. We find that λ_5 is negative when $\alpha=0$ or in the regions

$$0 < \alpha \quad \land \quad \beta < -\frac{\alpha}{3} + \frac{2}{3}\sqrt{\frac{36 + \alpha^4}{\alpha^2}}, \tag{31}$$

$$\alpha < 0 \quad \land \quad \beta > -\frac{\alpha}{3} - \frac{2}{3}\sqrt{\frac{36 + \alpha^4}{\alpha^2}}.$$
 (32)

Therefore, (DE-I) is an attractor in these regions. By looking at Eqs. (19)-(23), we note that the autonomous system possesses the symmetry $\{x \to -x, \alpha \to -\alpha, \beta \to -\beta\}$, which we can see it is obeyed in Fig. 3 and also in the regions in Eqs. (31) and (32).

D. Numerical Fixed points

In order to simplify our numerical treatment, we will assume that radiation is negligible; i.e. $\Omega_r = 0$. Besides the solutions given above, it can be shown

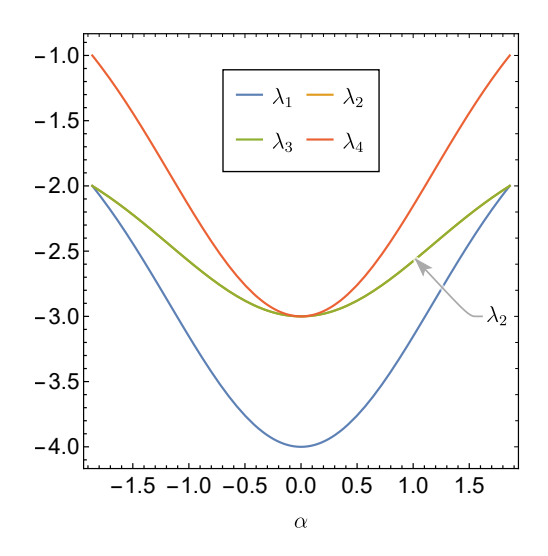


FIG. 2. Eigenvalues of the Jacobian matrix evaluated at (DE-I). Note that $\lambda_{1,2,3,4} < 0$ in the whole region where (DE-I) is an accelerated solution; i.e. $w_{\text{eff}} < -1/3$.

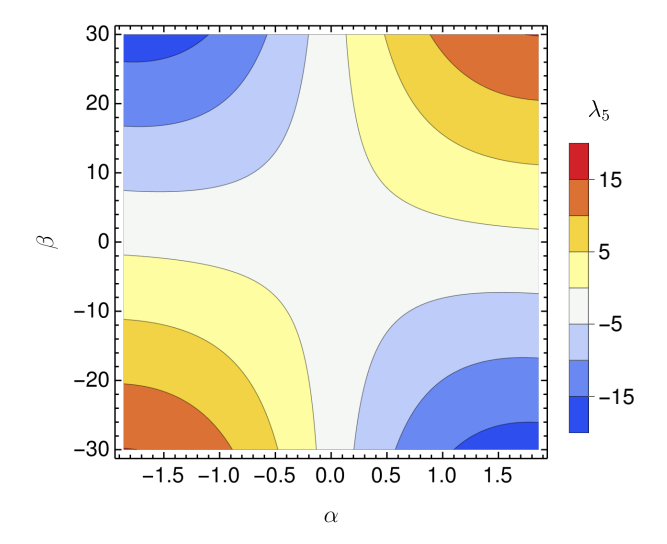


FIG. 3. Eigenvalue of the Jacobian matrix evaluated at (DE-I). This eigenvalue is negative in the regions given in Eqs. (31) and (32).

that there are no more analytical fixed points cosmologically viable. Replacing in the autonomous system, Eqs. (19)-(22), the expression of the deceleration parameter q in terms of the variables, Eq. (13), and making derivatives equal to zero, it is possible to

simplify the resulting algebraic system as

$$0 = \alpha^{2}y^{4} + 2\sqrt{3}\alpha xy^{3} + 3x^{2}y^{2} + \beta^{2}x^{2}z^{4} - \beta^{2}z^{4},$$

$$(33)$$

$$0 = 9(x^{2} - 1)y^{4} + 2\sqrt{3}\alpha x(3\Sigma^{2} + z^{2} + 3)y \quad (34)$$

$$+ 3\alpha^{2}x^{2}y^{2} + (3\Sigma^{2} + z^{2} + 3)^{2},$$

$$0 = 9(x^{2} - 1)y^{4} + (\Sigma(3\Sigma - 4) + z^{2} - 1)^{2} \quad (35)$$

$$+ 3\beta^{2}x^{2}y^{2} - 2\sqrt{3}\beta x(\Sigma(3\Sigma - 4) + z^{2} - 1)y,$$

$$0 = 9\Sigma^{6} + (6z^{2} - 18)\Sigma^{4} + 24z^{2}\Sigma^{3} + 16z^{4} \quad (36)$$

$$+ (9(x^{2} - 1)y^{4} + z^{4} - 6z^{2} + 9)\Sigma^{2}$$

$$+ (8z^{2} - 24)z^{2}\Sigma.$$

These equations compose a polynomial system of degree greater than 4, since Eq. (36) is an equation of degree 6 in the variable Σ . This means that the system is not analytically solvable in general due to fundamental theorem of Galois theory [53]. Note that in the case $\Sigma = 0$, the degree of the system is reduced to 4 and thus analytical solutions exist, from which we showed the cosmologically relevant solutions in Eqs. (27) and (29).

Therefore, we proceed with the numerical procedure explained in Sec. II. Firstly, we have to choose a specific window parameter where the stochastic search will be performed. Having in mind that $|\alpha| < 1.86121$ for (DE-I) being an accelerated solution, we choose $\alpha \in [-30,30]$ and $\beta \in [0,30]$. Secondly, in order to get physically viable solutions, we impose the conditions

$$0 \le \Omega_m \le 1, \quad 0 \le \Omega_{\rm DE} \le 1. \tag{37}$$

Therefore, scattered points in the parameter space are cataloged as non-viable solutions if they do not obey these physical constraints. We call the viable region as (DE-II). We found that the curve dividing (DE-II) from non-viable points is given by

$$\beta = -\frac{\alpha}{3} + \frac{2}{3}\sqrt{\frac{36 + \alpha^4}{\alpha^2}},\tag{38}$$

which is the same curve dividing the regions where (DE-I) is an accelerated solution [see Eqs. (31) and (32)]. Having the existence region for (DE-II), now we ask if there exist accelerated solutions in this region. The color-plot in Fig. 4 shows that the viable region can be divided in accelerated and non-accelerated solutions by the line $w_{\rm eff}(\alpha,\beta)=-1/3$. Therefore, we can assure the existence of a DE dominated solution, either isotropic or anisotropic, for any pair of α and β .

The stability of (DE-II) has to be analyzed numerically. Hence, we compute the sign of the

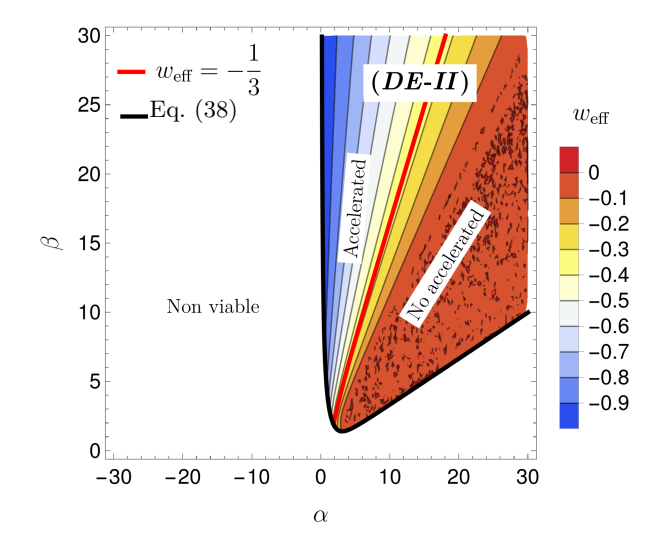


FIG. 4. Values of $w_{\rm eff}$ in (DE-II). The red line is $w_{\rm eff} = -1/3$ divides (DE-II) in two regions: one is for accelerated solutions, and the other one for non-accelerated solutions.

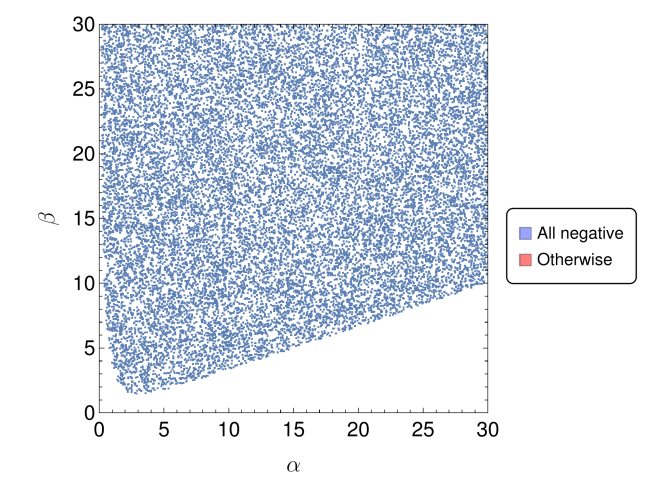


FIG. 5. Sign of eigenvalues of the Jacobian matrix in (DE-II). A blue point represents when all the eigenvalues are negative. In this case, the blue region is the same region of existence of (DE-II); i.e. whenever (DE-II) exists, it is an attractor.

eigenvalues of the Jacobian matrix in this point. As shown in Fig. 5, (DE-II) is an attractor in its region of existence. Therefore, if this points exists, then it is the only attractor of the system.

The code for simulating 10000 points in the specified region, or equivalently solving 10000 dynamical systems, takes approximately 45 minutes running on 136 parallelized mixed physical cores. The code will

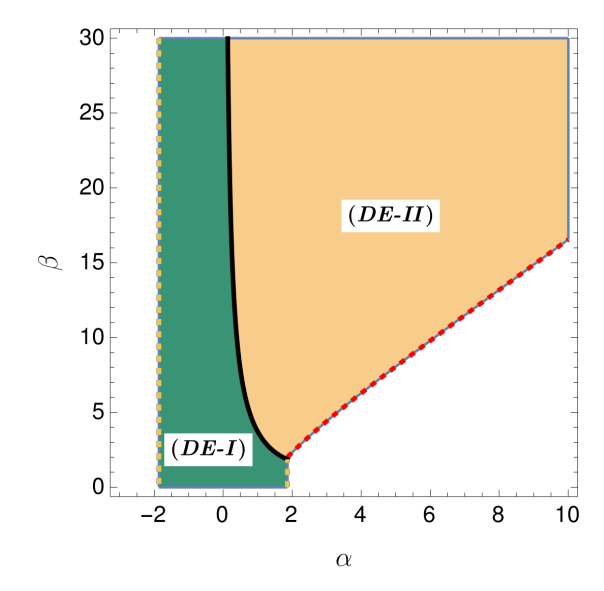


FIG. 6. Regions where (DE-I) and (DE-II) are attractors and accelerated solutions. The black line is the bifurcation curve given in Eq. (38).

be available on GitHub.⁵

IV. NUMERICAL INTEGRATION OF THE AUTONOMOUS SET

In order to check our claims about the asymptotic behavior of the system, in this section we numerically solve the full system in Eqs. (19) - (23) for specific values of α and β . We assume an initially smooth Universe; i.e. $\Sigma_i = 0$. Furthermore, the initial conditions are set at a very high redshift $z_r = 6.57 \times 10^7$, ensuring that cosmological trajectories start in the deep radiation epoch. In particular we choose

$$x_i = 10^{-25}, \quad z_i = 10^{-15}, \quad \Omega_{r_i} = 0.99995.$$
 (39)

The value for y_i is constrained by Eq. (7). For $0 \le \Omega_{m_i} \le 1$, y_i have to satisfy $|y_i| \le 0.00707$, so we choose

$$y_i = 2.01 \times 10^{-14},\tag{40}$$

such that $\Omega_{m_i} = 5.0 \times 10^{-5}$. We would like to point out that the values of x_i , z_i , and y_i are chosen so small to avoid possible large contributions of dark energy during the radiation dominated epoch.

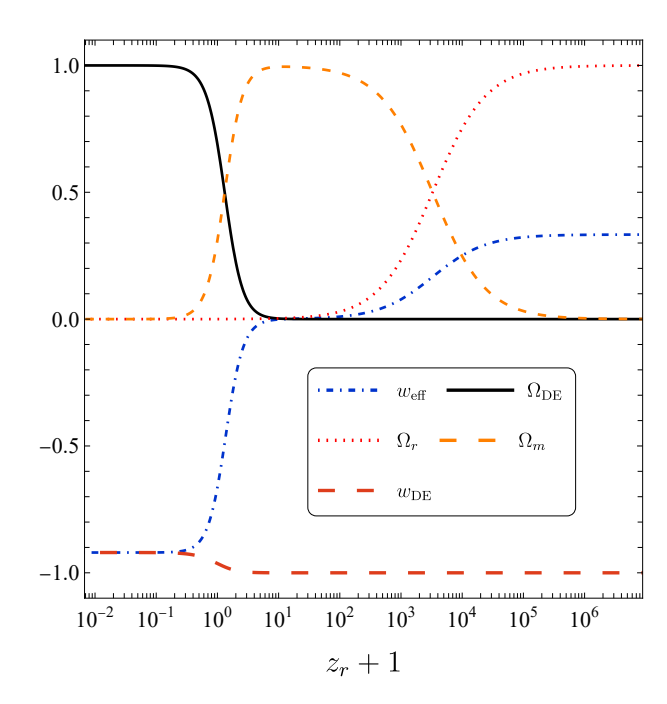


FIG. 7. Evolution of the density parameters, $w_{\rm eff}$ and $w_{\rm DE}$ during the whole expansion history. The initial conditions, Eq. (39), were chosen in the deep radiation era at the redshift $z_r = 6.57 \times 10^7$. The universe passes through radiation dominance at early times (red dotted line), followed by a matter dominance (light brown dashed line), and ends in the DE dominance (black solid line) characterized by $w_{\rm eff} = w_{\rm DE} \approx -1$ (blue dot-dashed line and tangelo dashed line, respectively).

A. Isotropic Dark Energy Attractor

Firstly, we choose α and β such that (DE-I) is the attractor of the system:

$$\alpha = 0.5, \quad \beta = 0.1,$$
 (41)

In FIG. 7. we plotted the evolution of the density parameters, the effective equation of state of the universe and the equation of state of DE as function of the redshift z_r . We can see that the early universe $(z_r > 10^6)$ is dominated by radiation (red dotted line). Then, at $z_r \approx 3200$, we have radiation-tomatter transition, that is $\Omega_m \simeq \Omega_r$. During this we have $\Omega_{\rm DE} \approx 9.89 \times 10^{-10}$, obeying the BBN constraint $\Omega_{\rm DE} < 0.045$ at $z_r = 1200$. From this transition to $z_r \approx 0.3$, the Universe is dominated by matter (light brown dashed line). The contribution of DE to the energy budget at $z_r = 50$ is $\Omega_{\rm DE} = 1.74 \times 10^{-5}$, such that the value is in agreement with the CMB constraint $\Omega_{\rm DE} < 0.02$ at this redshift [4, 7, 54, 55]. After this point, DE dominates (black solid line). The ex-

 $^{^{5}\ \}mathrm{https://github.com/sagaser/Numerical-dynamical-analysys}$

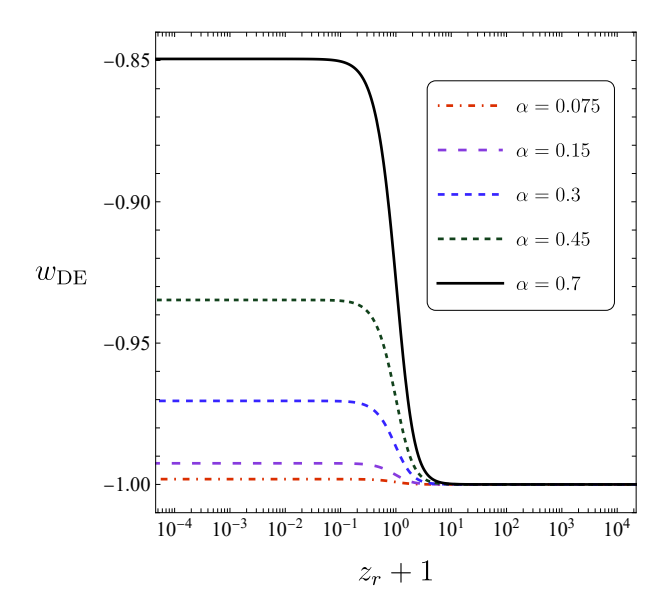


FIG. 8. At left hand we have late-time evolution of the dark energy equation of state $w_{\rm DE}$ for different values of the parameter α , while $\beta = -90$ is fixed, at right hand we have the time evolution of the dark energy equation of state for different values of the parameter β , while $\alpha = 0.5$ is fixed and for both graphs the initial conditions are the same given in Eq. (39).

pansion of the Universe speeds up since $w_{\rm eff} < -1/3$ (blue dot-dashed line). Note that the behavior of the equation of state of DE is in perfect agreement with what expected; i.e. it is equal to -1 during the radiation and matter epochs, and takes on a different value during the DE domination. This value depends only on α and in this case is given by $w_{\rm eff} = w_{\rm DE} \simeq -0.88$. In Fig. 8 we plot $w_{\rm DE}$ for several values of α and β fixed, where we can see that $w_{\rm DE} \to -1$ when $\alpha \to 0$ as expected.

We want to point out that we verified that $w_{\rm DE}$ does not depend on β and also that the shear $\Sigma=0$ during the whole expansion history. This had to be so, since (DE-II) does not exist when (DE-I) is an attractor. However, the conversely is not true. In general, when (DE-II) is the attractor of the system, (DE-I) exist as a saddle and the Universe could expand isotropically during a brief period of time.

B. Anisotropic Dark Energy Attractor

For (DE-II) to be the attractor of the system, we choose the following parameters

$$\alpha = 0.5, \quad \beta = 80, \tag{42}$$

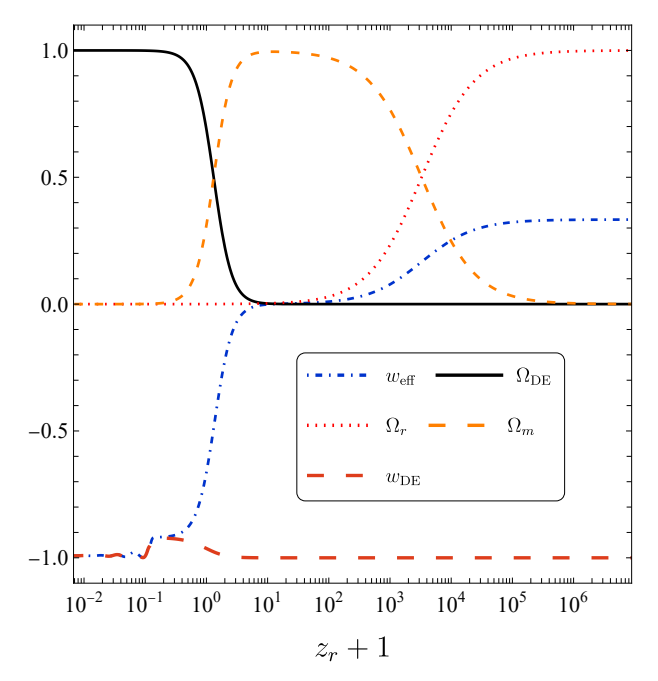
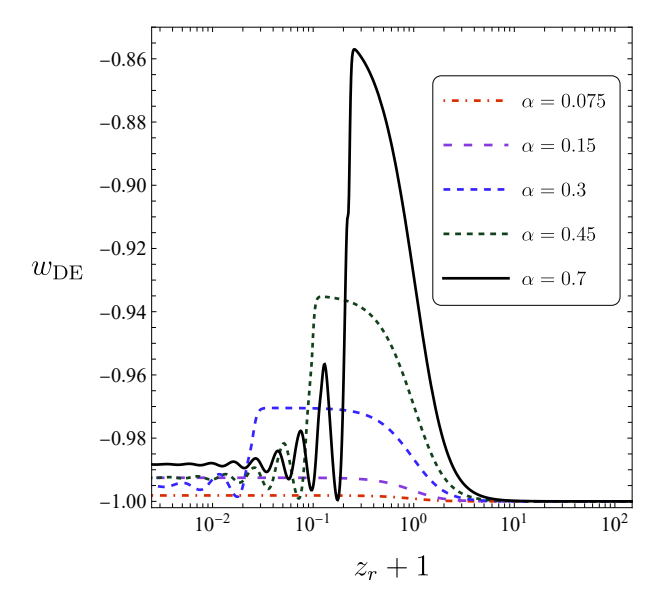


FIG. 9. Evolution of the density parameters, $w_{\rm eff}$ and $w_{\rm DE}$ during the whole expansion history. The initial conditions are the same as in Fig. 7. The only appreciable difference with respect to the evolution shown in Fig. 7 is that $w_{\rm eff} = w_{\rm DE} \approx -1$ oscillates at late times.

and we use the same initial conditions as in Eq. (39).

In Fig. 9, we plot the evolution of the density parameters, the effective equation of state and the equation of state of the DE as function of the redshift z_r . One difference with respect to Fig. 7 is worth noting, the oscillatory behavior of $w_{\rm DE}$ at late times. As mention in Ref. [47], these oscillations occur when the kinetic term of the scalar field is comparable to the vector density, turning the equation of motion of the scalar field (Eq. (9) in this case) into an equation describing a damped harmonic oscillator.

In Fig. 10, we plot the late-time evolution of $w_{\rm DE}$ and Σ for fixed $\beta=80$ and varying the parameter α . We observed that both $w_{\rm DE}$ and Σ oscillate until they stabilize to the value predicted in the numerical fixed point (DE-II), as shown in Table I. Note that the amplitude of these oscillations grows with α . We also investigate the behavior of $w_{\rm DE}$ and Σ when α is fixed and β varies, as shown in Fig. 11. In this case, the amplitude of the oscillations grows while β decreases. Note in Fig. 10 that when $w_{\rm DE}$ deviates from -1 it grows until a value which mainly depends on α . This is the indication that the Universe is crossing by the (DE-I) which is a saddle. When α is fixed as in Fig. 11, the time spent by the Universe crossing



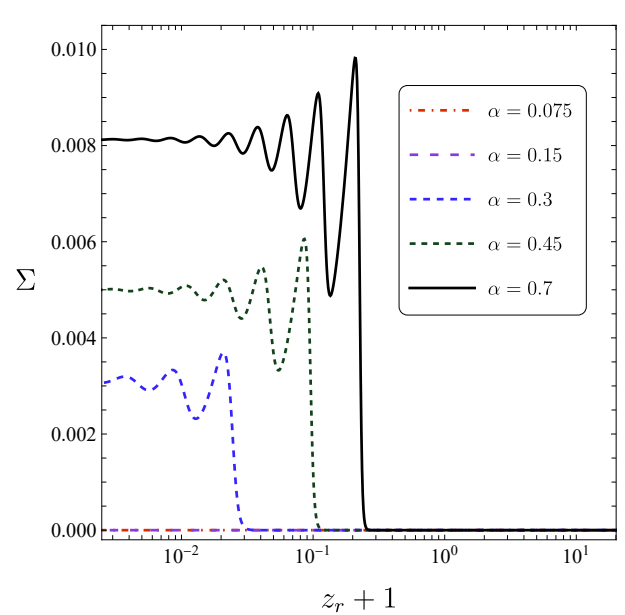


FIG. 10. Late-time evolution $(z_r < 10)$ of the equations of state of DE $w_{\rm DE}$ and the shear Σ for different values of the parameter α , while $\beta = 80$. The initial conditions are the same given in Eq. (39). Note that the amplitude of the oscillations is greater for greater α . As $w_{\rm DE}$ as Σ oscillate until they reach the asymptotical value predicted by the numerical fixed point (DE-II).

(*DE-I*) depends on β . For larger values of β , the coupling between the tachyon field and the vector field is stronger, and thus oscillations start earlier.

At this point, we would like to stress that the analysis presented in this section serves as a check for the asymptotic behavior predicted from the numeri-

TABLE I. Predicted values of Σ and $w_{\rm DE}$ as a function of each α and β in the region where the numerical approach was applied and solved with a mean error of 20% in Σ .

α	β	$\Sigma \times 10^{-3}$	$w_{ m DE}$
0.5	50	(5.58 ± 2.70)	-0.9867
0.5	70	(4.21 ± 0.46)	-0.9905
0.5	110	(2.81 ± 0.56)	-0.9939
0.5	250	(1.29 ± 0.61)	-0.9973
0.5	800	(41.2 ± 25.1)	-0.9992
0.075	80	(20.8 ± 0.1)	-0.9988
0.15	80	(83.3 ± 0.1)	-0.9975
0.3	80	(2.08 ± 0.56)	-0.9950
0.45	80	(3.33 ± 0.46)	-0.9925
0.7	80	(5.40 ± 2.70)	-0.9884

cal fixed point (*DE-II*). Hence, it establishes the consistency of the numerical method proposed in this work, and its usefulness when the cosmological viable parameter space of a model has no analytic description.

V. CONCLUSIONS

In this work, we have put forward a numerical method to find the cosmological viable parameter space of a model. We applied our method to a specific model of anisotropic dark energy based on the interaction between a tachyon field and a vector field. We have explicitly shown that the anisotropic attractor of the system has no analytical description, given that the degree of the algebraic system from which this point must be computed is greater than 4 [see Eqs. (33)-(36)]. However, when the anisotropy is neglected, the system is reduced to a system of degree 4 and thus analytical solutions exist, which we presented in Eqs. (27) and (29). In particular, our method allowed us to find the parameter space of the model where anisotropic accelerated solutions exist. which we plot in Fig. 4. Then, we checked the consistency of the method by numerically solve the full autonomous system in Eqs. (19)-(23) for a particular set of initial conditions. As a last remark, we would like to stress on the generality of our method, as explained in Sec. II; i.e. in principle, it can be applied to any DE scenario and we chose a particular model just for exemplifying purposes.

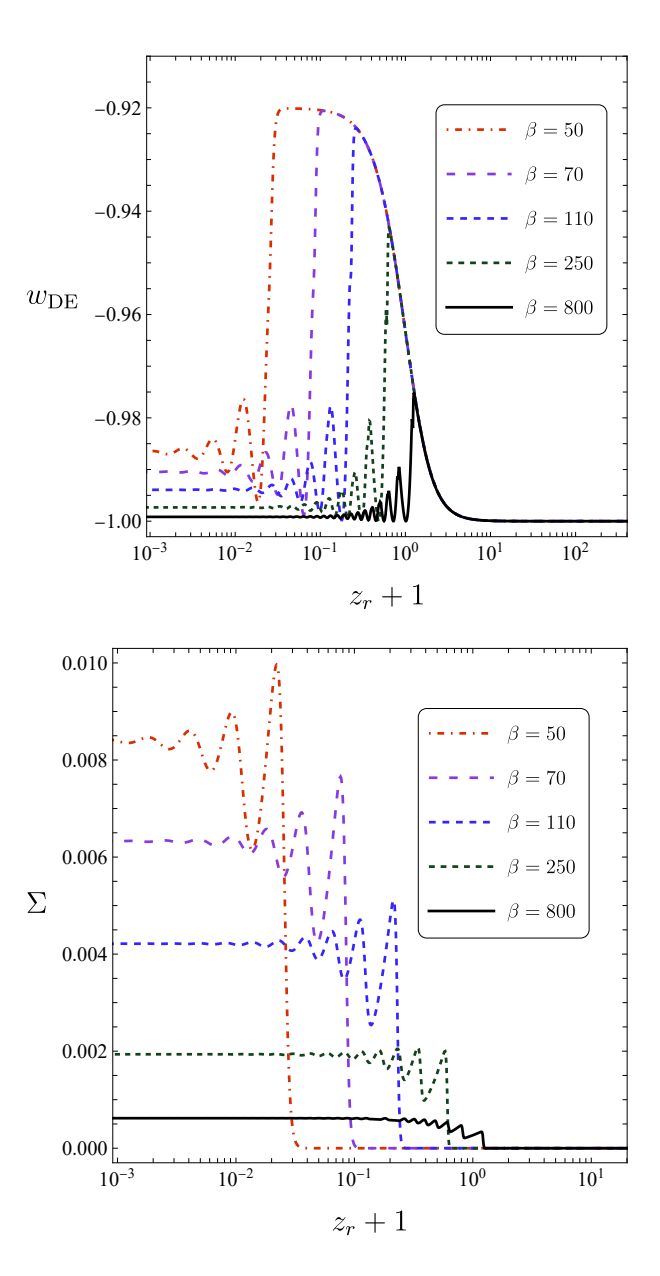


FIG. 11. Late-time evolution $(z_r < 10)$ of the equations of state of DE $w_{\rm DE}$ and the shear Σ for different values of the parameter β , while $\alpha = 0.5$. The initial conditions are the same given in Eq. (39). Note that the amplitude of the oscillations is greater for smaller β . As $w_{\rm DE}$ as Σ oscillate until they reach the asymptotical value predicted by the numerical fixed point (DE-II).

ACKNOWLEDGEMENTS

This work was supported by Patrimonio Autónomo - Fondo Nacional de Financiamiento para la Ciencia, la Tecnología y la Innovación Francisco José de

Caldas (MINCIENCIAS - COLOMBIA) Grant No. $110685269447~\mathrm{RC\text{-}}80740\text{-}}465\text{-}202,$ projects 69723 and 69553.

Appendix A: (DE-I) Eigenvalues

The eigenvalues for the isotropic DE, section III C are given by

$$\lambda_1 = \frac{1}{12} \left(-\sqrt{2}\sqrt{\alpha^4 + 36\Gamma} + \sqrt{2}\alpha^2\Gamma - 12 \right) \tag{A1}$$

$$\lambda_2 = \frac{1}{24} \left(-\sqrt{2}\sqrt{\alpha^4 + 36}\Gamma + \sqrt{2}\alpha^2\Gamma - 36 \right) \tag{A2}$$

$$\lambda_{3} = \frac{1}{48} \left(-36 + 3\sqrt{2}\alpha^{2}\Gamma - 3\sqrt{2}\sqrt{36 + \alpha^{4}}\Gamma \right)$$

$$-2\left(66\alpha^{8} + \alpha^{6} \left(-66\sqrt{36 + \alpha^{4}} + 32\sqrt{2}\Gamma \right) + \alpha^{2} \left(-900\sqrt{36 + \alpha^{4}} + 738\sqrt{2}\Gamma \right) \right)$$
(A3)

$$-162 \left(-36 + \sqrt{2} \sqrt{36 + \alpha^4} \Gamma\right) - 8\alpha^4 \left(-261 + 4\sqrt{2} \sqrt{36 + \alpha^4} \Gamma\right)\right)^{\frac{1}{2}}\right)$$

$$\lambda_4 = \frac{1}{48} \left(-36 + 3\sqrt{2}\alpha^2\Gamma - 3\sqrt{2}\sqrt{36 + \alpha^4}\Gamma + 2\left(66\alpha^8 + \alpha^6 \left(-66\sqrt{36 + \alpha^4} + 32\sqrt{2}\Gamma \right) + \alpha^2 \left(-900\sqrt{36 + \alpha^4} + 738\sqrt{2}\Gamma \right) \right)$$
(A4)

$$-162 \left(-36 + \sqrt{2} \sqrt{36 + \alpha^4} \Gamma\right) - 8\alpha^4 \left(-261 + 4\sqrt{2} \sqrt{36 + \alpha^4} \Gamma\right)^{\frac{1}{2}}\right)$$

$$\lambda_5 = \frac{1}{24} \left(2\sqrt{\alpha^4 + 36\alpha\beta} - \sqrt{2}\sqrt{\alpha^4 + 36\Gamma} - 2\alpha^3\beta + \sqrt{2}\alpha^2\Gamma - 12 \right)$$
(A5)

where $\Gamma \equiv \sqrt{\alpha^4 - \sqrt{\alpha^4 + 36\alpha^2 + 18}}$, $\lambda_1, \dots, \lambda_4$ are all negative if α is a real number, and λ_5 is negative

when Eq. (31) or Eq. (32) are satisfied.

- A. G. Riess et al. (Supernova Search Team), "Observational evidence from supernovae for an accelerating universe and a cosmological constant," Astron. J. 116, 1009–1038 (1998), arXiv:astro-ph/9805201.
- [2] S. Perlmutter *et al.* (Supernova Cosmology Project), "Measurements of Ω and Λ from 42 high redshift supernovae," Astrophys. J. **517**, 565–586 (1999), arXiv:astro-ph/9812133.
- [3] B. P. Schmidt et al. (Supernova Search Team), "The High Z supernova search: Measuring cosmic deceleration and global curvature of the universe using type Ia supernovae," Astrophys. J. 507, 46–63 (1998), arXiv:astro-ph/9805200.
- [4] M. Tegmark et al. (SDSS), "Cosmological parameters from SDSS and WMAP," Phys. Rev. D 69, 103501 (2004), arXiv:astro-ph/0310723.
- [5] M. Tegmark et al. (SDSS), "Cosmological Constraints from the SDSS Luminous Red Galaxies," Phys. Rev. D 74, 123507 (2006), arXiv:astro-ph/0608632.
- [6] D. N. Spergel *et al.* (WMAP), "First year Wilkinson Microwave Anisotropy Probe (WMAP) observations:

- Determination of cosmological parameters," Astrophys. J. Suppl. **148**, 175–194 (2003), arXiv:astroph/0302209.
- [7] N. Aghanim et al. (Planck), "Planck 2018 results.
 VI. Cosmological parameters," Astron. Astrophys. 641, A6 (2020), [Erratum: Astron.Astrophys. 652, C4 (2021)], arXiv:1807.06209 [astro-ph.CO].
- [8] E. Aubourg et al., "Cosmological implications of baryon acoustic oscillation measurements," Phys. Rev. D 92, 123516 (2015), arXiv:1411.1074 [astro-ph.CO].
- [9] W. J. Percival et al., "Measuring the Baryon Acoustic Oscillation scale using the SDSS and 2dFGRS," Mon. Not. Roy. Astron. Soc. 381, 1053–1066 (2007), arXiv:0705.3323 [astro-ph].
- [10] P. de Bernardis et al. (Boomerang), "A Flat universe from high resolution maps of the cosmic microwave background radiation," Nature 404, 955–959 (2000), arXiv:astro-ph/0004404.
- [11] A. H. Jaffe et al., "Recent results from the maxima experiment," New Astron. Rev. 47, 727–732 (2003), arXiv:astro-ph/0306504.

- [12] L. Perivolaropoulos and F. Skara, "Challenges for ΛCDM: An update," New Astron. Rev. 95, 101659 (2022), arXiv:2105.05208 [astro-ph.CO].
- [13] A. G. Riess et al., "A Comprehensive Measurement of the Local Value of the Hubble Constant with 1 km s⁻¹ Mpc⁻¹ Uncertainty from the Hubble Space Telescope and the SH0ES Team," Astrophys. J. Lett. 934, L7 (2022), arXiv:2112.04510 [astro-ph.CO].
- [14] W. L. Freedman, "Measurements of the Hubble Constant: Tensions in Perspective," Astrophys. J. 919, 16 (2021), arXiv:2106.15656 [astro-ph.CO].
- [15] E. Abdalla et al., "Cosmology intertwined: A review of the particle physics, astrophysics, and cosmology associated with the cosmological tensions and anomalies," JHEAp 34, 49–211 (2022), arXiv:2203.06142 [astro-ph.CO].
- [16] R. A. Battye, T. Charnock, and A. Moss, "Tension between the power spectrum of density perturbations measured on large and small scales," Phys. Rev. D 91, 103508 (2015).
- [17] M. Gatti et al., "Dark Energy Survey Year 3 results: cosmology with moments of weak lensing mass maps," (2021), arXiv:2110.10141 [astro-ph.CO].
- [18] E. Macaulay, I. K. Wehus, and H. K. Eriksen, "Lower growth rate from recent redshift space distortion measurements than expected from planck," Phys. Rev. Lett. 111, 161301 (2013).
- [19] D. Zürcher et al., "Dark Energy Survey Year 3 results: Cosmology with peaks using an emulator approach," (2021), arXiv:2110.10135 [astro-ph.CO].
- [20] A. Blanchard and S. Ilić, "Closing up the cluster tension?" (2021), arXiv:2104.00756 [astro-ph.CO].
- [21] L. Huang, Z. Huang, H. Zhou, and Z. Li, "The S₈ Tension in Light of Updated Redshift-Space Distortion data," (2021), arXiv:2110.08498 [astro-ph.CO].
- [22] C. Heymans et al., "KiDS-1000 Cosmology: Multiprobe weak gravitational lensing and spectroscopic galaxy clustering constraints," Astron. Astrophys. 646, A140 (2021), arXiv:2007.15632 [astro-ph.CO].
- [23] C. Chang et al. (DES, SPT), "Joint analysis of DES Year 3 data and CMB lensing from SPT and Planck II: Cross-correlation measurements and cosmological constraints," (2022), arXiv:2203.12440 [astroph.CO].
- [24] C. L. Bennett et al., "Seven-Year Wilkinson Microwave Anisotropy Probe (WMAP) Observations: Are There Cosmic Microwave Background Anomalies?" Astrophys. J. Suppl. 192, 17 (2011), arXiv:1001.4758 [astro-ph.CO].
- [25] L. Perivolaropoulos, "Large Scale Cosmological Anomalies and Inhomogeneous Dark Energy," Galaxies 2, 22–61 (2014), arXiv:1401.5044 [astro-ph.CO].
- [26] D. J. Schwarz, C. J. Copi, D. Huterer, and G. D. Starkman, "CMB Anomalies after Planck," Class. Quant. Grav. 33, 184001 (2016), arXiv:1510.07929 [astro-ph.CO].
- [27] Y. Akrami et al. (Planck), "Planck 2018 results. VII. Isotropy and Statistics of the CMB," Astron. Astrophys. 641, A7 (2020), arXiv:1906.02552 [astroph.CO].

- [28] Y. Akrami et al. (Planck), "Planck 2018 results. IX. Constraints on primordial non-Gaussianity," Astron. Astrophys. 641, A9 (2020), arXiv:1905.05697 [astro-ph.CO].
- [29] E. Di Valentino, A. Melchiorri, and O. Mena, "Can interacting dark energy solve the H_0 tension?" Phys. Rev. D **96**, 043503 (2017), arXiv:1704.08342 [astro-ph.CO].
- [30] R. Y. Guo, J. F. Zhang, and X. Zhang, "Can the H_0 tension be resolved in extensions to Λ CDM cosmology?" JCAP **02**, 054 (2019), arXiv:1809.02340 [astro-ph.CO].
- [31] E. Di Valentino et al., "In the realm of the Hubble tension — a review of solutions," Class. Quant. Grav. 38, 153001 (2021), arXiv:2103.01183 [astro-ph.CO].
- [32] L. Heisenberg, H. Villarrubia-Rojo, and J. Zosso, "Simultaneously solving the H_0 and σ_8 tensions with late dark energy," (2022), arXiv:2201.11623 [astroph.CO].
- [33] E. J. Copeland, M. Sami, and S. Tsujikawa, "Dynamics of dark energy," Int. J. Mod. Phys. D 15, 1753–1936 (2006), arXiv:hep-th/0603057.
- [34] J. Wainwright and G. F. R. Ellis, *Dynamical Systems in Cosmology* (Cambridge University Press, New York, 2009).
- [35] R. García-Salcedo, T. Gonzalez, F. A. Horta-Rangel, I. Quiros, and D. Sanchez-Guzmán, "Introduction to the application of dynamical systems theory in the study of the dynamics of cosmological models of dark energy," Eur. J. Phys. 36, 025008 (2015), arXiv:1501.04851 [gr-qc].
- [36] S. Smale, *Dynamical systems* (American Mathematical Soc., 2012).
- [37] R. L. Devaney, A first course in chaotic dynamical systems: theory and experiment (CRC Press, 2018).
- [38] M. Brin and G. Stuck, Introduction to dynamical systems (Cambridge University Press, 2013).
- [39] S. Bahamonde et al., "Dynamical systems applied to cosmology: dark energy and modified gravity," Phys. Rept. 775-777, 1–122 (2018), arXiv:1712.03107 [gr-qc].
- [40] M. Álvarez, J. B. Orjuela-Quintana, Y. Rodriguez, and C. A. Valenzuela-Toledo, "Einstein Yang-Mills Higgs dark energy revisited," Class. Quant. Grav. 36, 195004 (2019), arXiv:1901.04624 [gr-qc].
- [41] A. Guarnizo, J. B. Orjuela-Quintana, and C. A. Valenzuela-Toledo, "Dynamical analysis of cosmological models with non-Abelian gauge vector fields," Phys. Rev. D 102, 083507 (2020), arXiv:2007.12964 [gr-qc].
- [42] J. Motoa-Manzano, J. Bayron Orjuela-Quintana, Thiago S. Pereira, and C. A. Valenzuela-Toledo, "Anisotropic solid dark energy," Phys. Dark Univ. 32, 100806 (2021), arXiv:2012.09946 [gr-qc].
- [43] J. B. Orjuela-Quintana, M. Alvarez, C. A. Valenzuela-Toledo, and Y. Rodriguez, "Anisotropic Einstein Yang-Mills Higgs Dark Energy," JCAP 10, 019 (2020), arXiv:2006.14016 [gr-qc].
- [44] A. De Felice et al., "Cosmology in generalized Proca theories," JCAP 06, 048 (2016), arXiv:1603.05806

- [gr-qc].
- [45] S. Basilakos, G. Leon, G. Papagiannopoulos, and E. N. Saridakis, "Dynamical system analysis at background and perturbation levels: Quintessence in severe disadvantage comparing to ΛCDM," Phys. Rev. D 100, 043524 (2019), arXiv:1904.01563 [gr-qc].
- [46] J. Ohashi, J. Soda, and S. Tsujikawa, "Anisotropic power-law k-inflation," Phys. Rev. D 88, 103517 (2013), arXiv:1310.3053 [hep-th].
- [47] J. B. Orjuela-Quintana and C. A. Valenzuela-Toledo, "Anisotropic k-essence," Phys. Dark Univ. 33, 100857 (2021), arXiv:2106.06432 [gr-qc].
- [48] J. M. Aguirregabiria et al., "Tracking solutions in tachyon cosmology," Phys. Rev. D 69, 123502 (2004), arXiv:hep-th/0402190.
- [49] W. R. L. Abramo and F. Finelli, "Cosmological dynamics of the tachyon with an inverse powerlaw potential," Phys. Lett. B 575, 165–171 (2003),

- ar Xiv: astro-ph/0307208.
- [50] J. S. Bagla et al., "Cosmology with tachyon field as dark energy," Phys. Rev. D 67, 063504 (2003), arXiv:astro-ph/0212198.
- [51] K. Nozari and N. Rashidi, "Some Aspects of Tachyon Field Cosmology," Phys. Rev. D 88, 023519 (2013), arXiv:1306.5853 [gr-qc].
- [52] S. Hussain et al., "Dynamical systems analysis of tachyon dark energy model from a new perspective," (2022), arXiv:2208.10352 [gr-qc].
- [53] L. Ribes and P. Zalesskii, "Free profinite groups," in Profinite Groups (Springer, 2010) pp. 75–118.
- [54] S. Tsujikawa L. Amendola, *Dark Energy: Theory and Observations* (Cambridge University Press, 2015).
- [55] J. Phillips, D. H. Weinberg, R. A. C. Croft, L. Hernquist, N. Katz, and Pettini M., "Constraints on cosmological parameters from the ly α forest power spectrum and COBEDMR," The Astrophysical Journal **560**, 15–27 (2001).